Electronic and Chemical Properties of Donor, Acceptor Centers in Graphene

Mykola Telychko,[†,‡] Pingo Mutombo,[†] Pablo Merino,[§] Prokop Hapala,[†] Martin Ondráček,[†] François C. Bocquet,[#,∥] Jessica Sforzini,[#,∥] Oleksandr Stetsovych,[†] Martin Vondráček,[⊥] Pavel Jelínek,[*,†] and Martin Švec[*,†]

[†]Institute of Physics, Academy of Sciences of the Czech Republic, Cukrovarnická 10, CZ 16200, Prague, Czech Republic, [‡]Faculty of Mathematics and Physics, Charles University, V Holešovičkách 2, Praha 8, Czech Republic, [§]Max Planck Institute for Solid State Research, Heisenberg Strasse 1, 70569 Stuttgart, Germany, [#]Peter Grünberg Institut (PGI-3), Forschungszentrum Jülich, 52425 Jülich, Germany, [∥]Jülich-Aachen Research Alliance (JARA); Fundamentals of Future Information Technology, 52425 Jülich, Germany, and [⊥]Institute of Physics, Academy of Sciences of the Czech Republic, Na Slovance 2, 10, CZ 18228, Prague, Czech Republic

ABSTRACT Chemical doping is one of the most suitable ways of tuning the electronic properties of graphene and a promising candidate for a band gap opening. In this work we report a reliable and tunable method for preparation of high-quality boron and nitrogen co-doped graphene on silicon carbide substrate. We combine experimental (dAFM, STM, XPS, NEXAFS) and theoretical (total energy DFT and simulated STM) studies to analyze the structural, chemical, and electronic properties of the single-atom substitutional dopants in graphene. We show that chemical identification of boron and nitrogen substitutional defects can be achieved in the STM channel due to the quantum interference effect, arising due to the specific electronic structure of nitrogen dopant sites. Chemical reactivity of single boron and nitrogen dopants is analyzed using force—distance spectroscopy by means of dAFM.

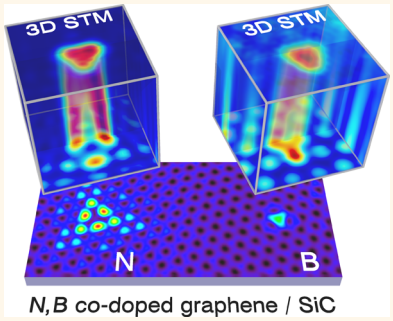

KEYWORDS: graphene · doping · boron · nitrogen · chemical reactivity

Chemical doping is among the most promising routes of tuning graphene's carrier densities for applications in nanoelectronics.[1−5] Boron (B) and nitrogen (N) atoms are the most suitable candidates for direct incorporation into the graphene honeycomb lattice, which result in an effective p- and n-doping, respectively.[6] Recent experimental and theoretical investigations discovered the possibility of band gap engineering by low-concentration BN-doping of graphene,[7−9] thus overcoming one of the major obstacles on the way toward applications in electronic devices. For graphene epitaxially grown on metallic substrates, doping is achieved by a standard chemical vapor deposition (CVD) method.[10] The dopant concentration can be controlled by adding gaseous precursors that contain the dopant during graphene growth.[11−15] This method was applied for preparation of BN-co-doped graphene as well.[7,16] A similar strategy has also been successful for N-doping of graphene grown on SiC substrates, by exposing the substrate to N_2 gas during the growth procedure.[17] An alternative doping method by ion implantation, which allows a better concentration control and purity of N-doping, was recently demonstrated.[18−24] On the other hand, a tunable B-doping or BN-co-doping of graphene on SiC has not been reported yet.

Here we report a procedure allowing the preparation of a stable B-doped and BN-co-doped single and bilayer graphene, epitaxially grown on the Si-face 6H-SiC(0001) substrate. Our technique yields B and N atoms substitutionary incorporated into the lattice, in the sp^2 electronic configuration. To investigate structural, chemical, and electronic properties of the B and N dopants in this system, we applied complementary experimental techniques. Scanning tunneling microscopy (STM) was employed to study the doping process and structural and electronic properties of individual dopants, while simultaneous dynamical atomic force microscopy (dAFM) provided measurements of short-range interactions with individual atoms. X-ray photoemission spectroscopy (XPS) and near-edge X-ray absorption fine structure spectroscopy (NEXAFS) provided additional information about the chemical environment of dopants in the graphene lattice. Results are supported by total energy density functional theory (DFT) and STM simulations.

* Address correspondence to pavel.jelinek@fzu.cz, svec@fzu.cz.

Received for review June 17, 2015 and accepted August 9, 2015.

Published online August 09, 2015
10.1021/acsnano.5b03690

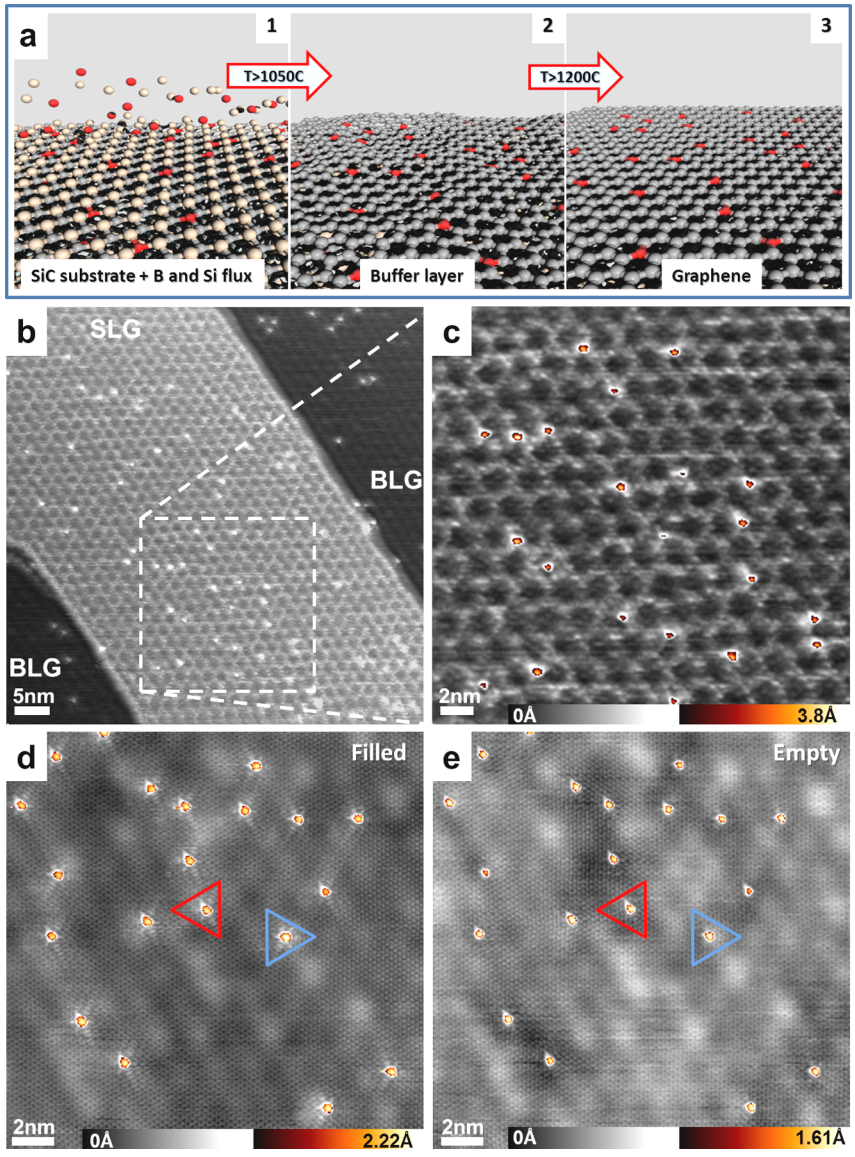

Figure 1. (a) Scheme of the preparation procedure of B-doped graphene on the SiC(0001) substrate. Gray, light brown, and red colors correspond to C, Si, and B atoms, respectively. (b) Large-scale STM image (−0.98 V, 0.2 nA, 60 × 60 nm^2) showing the presence of dopants in single- (SLG) and bilayer graphene (BLG) prepared following the procedure. (c) Magnified region of the B-doped SLG (−1.0 V, 0.2 nA, 25 × 25 nm^2). (d) Occupied and (e) empty state STM images (−0.5 and 0.5 V, 0.15 nA, 20 × 20 nm^2) of the B-doped BLG on 6H-SiC(0001). Red and blue triangles denote B dopants in the two inequivalent graphene sublattices.

RESULTS AND DISCUSSION

Figure 1a shows a scheme of the growth method that we applied to achieve the B-doping. First, the bare SiC(0001) substrate is cleaned *via* a Si flux and enriched with B atoms, which are deposited on the annealed sample. Boron atoms are introduced either by an e-beam evaporation or along with the Si flux from a heavily B-doped Si evaporation source during the growing process. Subsequent annealing above 1050 °C causes Si depletion and formation of the buffer layer with incorporated B atoms. Annealing of the sample further above 1200 °C leads to Si loss from the upper surface layers, thus transforming the buffer layer into the B-doped single- and bilayer graphene (SLG and BLG, respectively).

Figure 1b presents an STM overview image of the B-doped graphene grown on 6H-SiC(0001). A 40-nm-wide band of SLG is located between two BLG domains. Both SLG and BLG regions appear decorated with atomic-scale implants. We show a zoom-in on the SLG region in Figure 1c, which reveals randomly distributed single dopants and the typical modulation characteristic for the SLG grown on a SiC substrate.[6,25] The dopants are well separated from each other, and their prevalent locations are in the elevated areas of the modulation. The images in Figure 1d,e show the BLG region presenting a smaller corrugation due to a better decoupling from the substrate. This allows recognition of the dopants in two different orientations,

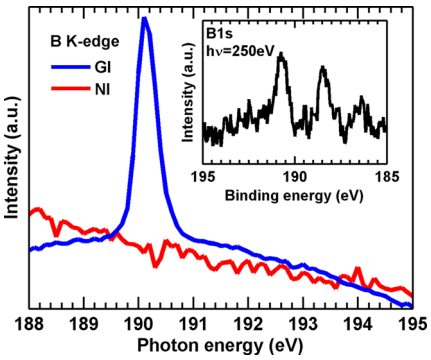

Figure 2. Absorption spectrum for the B K-edge, measured as B-KLL Auger electron yield. The inset shows the corresponding B 1s core level photoemission peaks. Blue and red curves correspond to grazing incidence (GI) and normal incidence (NI) geometries, respectively.

corresponding to the A and B sublattices of the graphene honeycomb structure.[26] The ratio between dopants in both sublattices is roughly 1:1. Comparison of the BLG images taken with negative and positive voltages on the tip (filled and empty states, Figure 1d and e, respectively) reveals a dark halo around the dopants in the empty states image. Noteworthy, the characteristic STM contrast of the dopants resembles that reported recently on the B-doped graphene grown by the CVD method on the Cu substrate.[14] The overall dopant concentration on SLG and BLG in this particular experiment was below 0.1% of the atoms forming the topmost graphene layer.

To corroborate the incorporation of the B into the graphene lattice and to determine its electronic configuration, we performed NEXAFS measurements. The absorption spectra for the B K-edge, measured as B-KLL Auger electron yield, are shown in Figure 2 for two geometries. The grazing incidence (GI) spectrum exhibits a sharp resonance at the photon energy of 190.1 eV. It is a clear signature of B electrons being a part of the graphene π system, similar to that observed previously for N dopants.[20] On the other hand, the normal incidence (NI) geometry yield does not present any strong dependence on the photon energy.

The spectra in both geometries support the interpretation that the surface contains a significant amount of B atoms hybridized with their C neighbors into the sp^2 configuration.

B is also detected in the core level spectrum (see inset of Figure 2). Here, two main components can be identified, at 190.6 and 188.2 eV. The appearance of more than one component suggests that B atoms are present on the surface in various bonding configurations. We assign the higher binding energy peak to the sp^2-hybridized B in the graphene and the lower binding energy peak to the B in the bulk.

The substitutional B dopants are remarkably stable in ambient conditions. No significant variations in the concentration or structure were observed after

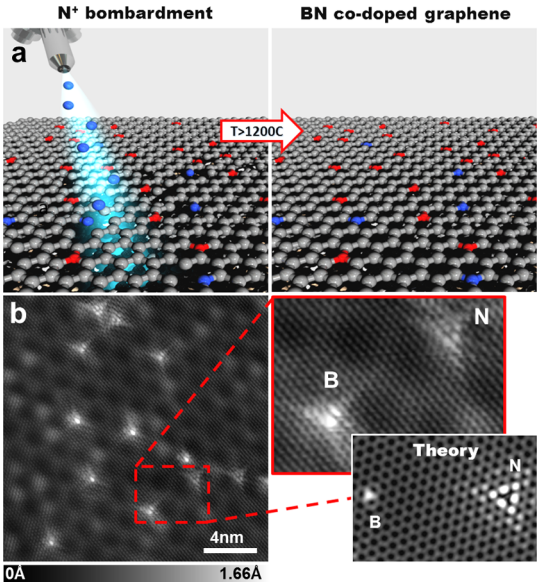

Figure 3. (a) Scheme of BN co-doping: N ion implantation into the previously B-doped sample and thermal stabilization. (b) Constant-current STM image showing presence of N and B dopants in the graphene lattice ($U = -0.7$ mV; $I = 0.15$ nA; 20×20 nm^2). The inset shows a zoomed-in area with a detail of N and B single-atom dopants and a simulated STM image for comparison.

exposing the samples to air for extended periods of time (more than 10 days). Annealing of the sample up to 800 °C under a 10^{-5} mbar CO and O_2 atmosphere did not induce any changes to graphene nor to the B dopants. Only after repeated annealing to temperatures above 1000 °C in ultrahigh vacuum (several hours in total) did we observe a reduction of the dopant concentration, in both STM and XPS measurements. Such an effect may be caused by diffusion of the B dopants deeper into the SiC bulk.

To explore the possibility of a BN co-doping and to compare the electronic properties of individual B and N dopants, we used the N implantation method known from previous works.[18,20] With this method, doping levels of both B and N atoms are adjustable. In the low concentration regime, we prepared first the B-doped graphene/SiC(0001) sample with a desired B dopant density by the previously described method. The sample was then exposed to N-ion flux and stabilized by annealing.[20] The graphical scheme in Figure 3a summarizes the procedure. The precise control over the N-doping concentration can be attained by changing the flux density and duration of the ion irradiation. For the B-doping control, the crucial factor is the amount of B deposited on the sample surface before the graphene growth (see Supporting Information).

In Figure 3b we show an atomically resolved STM scan of the surface after such treatment. Single-atom N dopants appear as triangular-shaped objects with pronounced depressions in the middle, whereas the B dopants possess a maximum intensity in the center. The observed STM contrast of N dopants agrees well

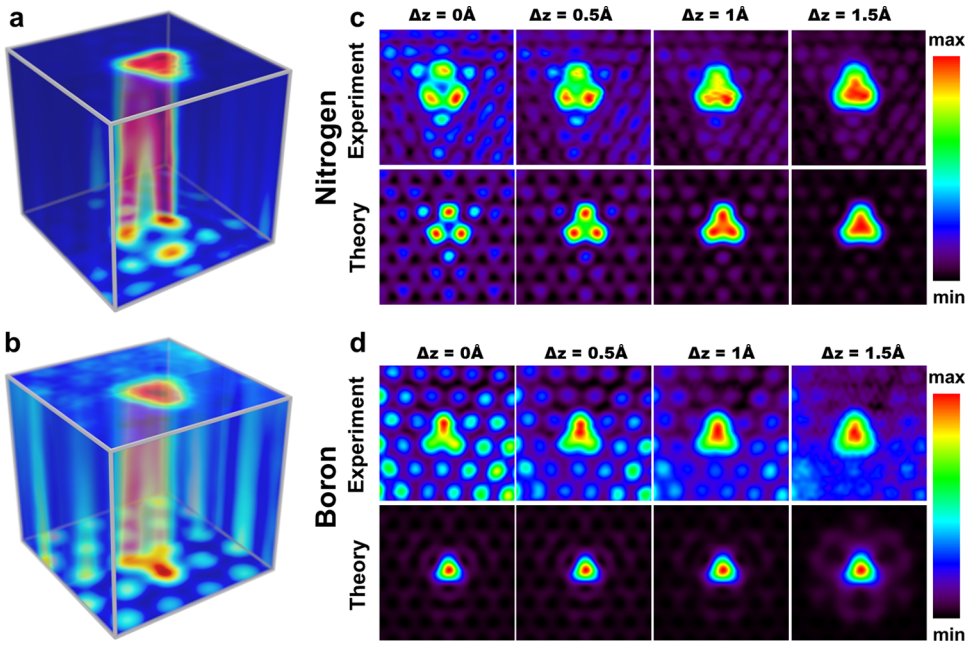

Figure 4. Representation of the 3D maps of tunneling current for (a) N dopant (−100 mV, 1.8 × 1.8 × 0.15 nm^3, I_{set} = 1 nA) and (b) B dopant (−150 mV, 1.8 × 1.8 × 0.15 nm^3, I_{set} = 1 nA). The 3D maps are normalized for each height step. (c and d) Selected slices from the 3D map, taken above the N and B dopant, respectively, compared with the STM simulations generated using a carbon tip for the corresponding tip−sample distance range.

with previous atomically resolved STM studies reporting a suppression of the tunneling current over the N site.[13,18,20] Previously we attributed this characteristic dip above N to the destructive interference effect.[20] In the case of the B-substitutional dopants, the absence of this effect allows an accurate chemical discrimination between the N and B species using the STM images. We should note that STM images of doped samples with different concentration contain only a negligible amount of other than substitutional defects (see discussion in the Supporting Information).

To gain more insight into the local chemical and electronic properties of B and N substitutional defects, we performed simultaneous dAFM/STM measurements at low temperature. We acquired 3D constant-height dAFM/STM maps over N and B dopants. The full sets consisted of images taken with 10 pm height increments, thus creating full 3D maps of the tunneling current (Figure 4a,b) and the frequency shift (not shown). The 3D scans for N and B dopants were taken during different experimental sessions; that is, the tip apex was not the same.

Figure 4a,b displays a 3D representation of normalized site-dependent tunneling current $I(z)$ as a function of the tip position over the N and B dopant, respectively. Corresponding constant-height STM images taken in selected tip−sample distances are shown in Figure 4c,d. We can clearly see suppression of the tunneling current over the N atom in the close tip−sample distance, while the maximum of the tunneling current signal is detected over the three nearest neighbor C atoms. In the case of the B-site, the maximum tunneling is always detected over the B dopant independently of the tip−sample distance. Such characteristic behavior of the atomic contrasts observed above the N and B dopants is robust, and it was repeatedly observed during several experimental sessions.

For better clarity, we also plot the variation of the tunneling current $I(z)$ over several distinct atomic positions on and around the N dopant site as shown in Figure 5a. The reference measurements on graphene, including first- and third-neighbor C-sites, follow a nearly ideal exponential decay, with the exception of the very close distances. In the close distances the exponential growth is slightly suppressed, likely due to the onset of multiple-scattering effects.[27]

On the other hand, the N-site curve deviates significantly from the exponential dependence, becoming almost flat in the tip−sample proximity. The crossing of the curves pertaining to the neighboring sites marks the onset of the destructive interference effect,[20] followed by the inversion of contrast. In the case of B dopant (Figure 5b), the decays extracted over the B-site and its neighborhood are not deviating much from the ideal exponential decay with the tunneling current of each curve. Here, any strong influence of the interference effect can be excluded. This substantial difference between N and B dopant allows unambiguous chemical identification of the dopants in STM images.

We carried out constant-height STM simulations of B and N defects at selected distances using a carbon tip model; see Figure 4. The calculated STM images mimic

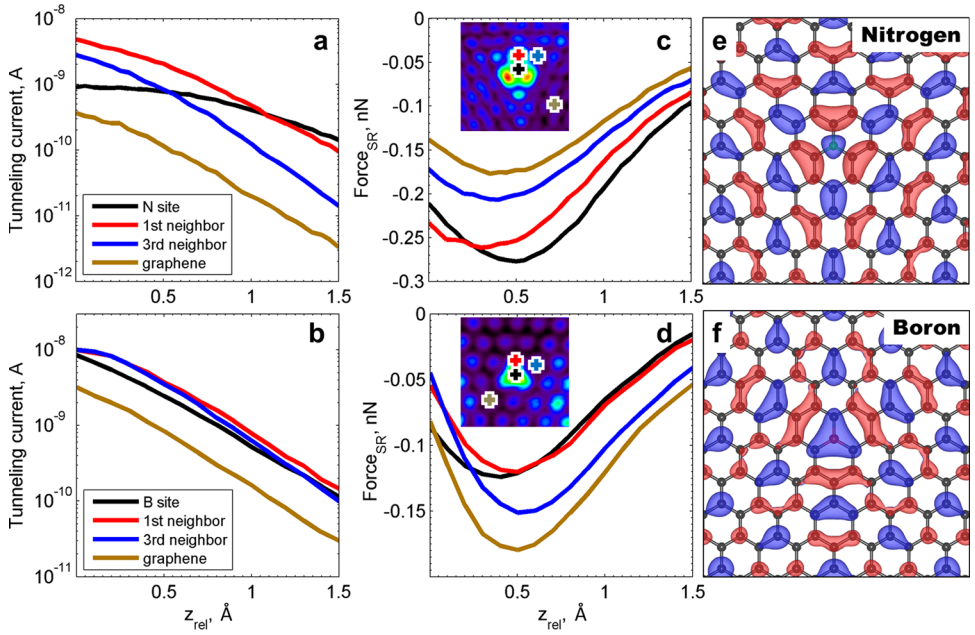

Figure 5. Experimental *I*(*z*) and *F*(*z*) spectroscopies taken at different positions over N dopant (a and c) and B dopant (b and d), with the insets denoting the measuremet sites. (e) Plot of the electronic state near the Fermi level for N dopant, showing the nodal structure in between N and the nearest C. (f) Plot of the electronic state near the Fermi level for B dopant.

very well not only the atomic contrast at given distance but also its variation with gradual change of the tip−sample distance. In the case of B dopant STM images can be interpreted in terms of surface local density of states. However, the atomic contrast observed for N dopant shows much more peculiar behavior, which cannot be explained only in terms of local density of states. Next, we will demonstrate that such an effect is driven by the quantum interference effect between different transport channels between the tip and sample.[20]

The excellent agreement between experimental evidence and calculated STM images together with the fact that the atomic contrast over B and N dopants is independent of tip apex indicates that the origin of the different atomic contrast is related to surface electronic structure. Thus, we analyzed the character of the electronic structure of B- and N-doped graphene relevant to the tunneling process near the Fermi level. Figure 5e and f represent the real space distribution of the electronic wave functions localized around the N and B dopants. We identify these two localized electronic states as significantly contributing to the tunneling current at low bias voltages. The most striking feature is that the wave function localized on the N-site has antibonding character with a characteristic node in between the central N atom and its nearest neighbor C atoms. The other way around, the B-site has bonding character with the same sign as its nearest neighbor C atoms. The presence of the node is the crucial factor giving rise to the destructive interference effect on the tunneling current above the N dopant site.[20] In particular, it causes the opposite signs of amplitudes, corresponding to transport eigenchannels passing from tip apex to N atom or the nearest neighbor C atoms, respectively. Consequently, this results in the suppression of the tunneling current observed over the N dopant.

The dAFM technique senses different kinds of long- and short-range forces simultaneously, acting between the tip and sample. Short-range forces appearing only in *z*-distances of a few angstroms are typically related to a local electrostatic or chemical interaction between the tip apex and surface atoms. In other words, the short-range forces acquired over different sites provide information about local chemical reactivity on different surface sites.[28,29] Therefore, 3D maps of the short-range force can provide further understanding of local chemical reactivity of doped graphene and the potential of the dopants as anchoring sites for graphene functionalization with organic molecules.[30−32]

Here we employ a 3D set of dAFM measurements to analyze the local interaction over B and N dopants. The measurements were done with two different tips with unknown chemical composition of the apex. Thus, we cannot compare directly the local interaction between B- and N-sites. Instead, we can compare variation of the short-range interaction with respect to pristine graphene. The short-range atomic forces extracted from the 3D map of the dAFM signal, obtained simultaneously with the tunneling current, are plotted for the same sites as the current in Figure 5d,e.

It is well known that pristine graphene shows a low chemical reactivity. Indeed we detected relatively small maximum attractive short-range forces, in the range of a few tenths of a nanonewton, over graphene during both

measurements; see yellow lines in Figure 5c,d. This indicates that the interaction between the tip apex and surface carbon atoms is governed by a weak electrostatic interaction, rather than by formation of a true chemical bond. Similarly, we found relatively weak, but different maximum attractive short-range forces over N- and B-sites. Since the previous findings corroborated that the dopants reside in the plane with graphene, the magnitudes of the maximum forces point toward their distinct local reactivity rather than a topographic effect. In the case of the N-site the maximum interaction is about 0.1 nN larger than over pristine graphene. In the case of the B dopant, we detect a smaller maximum attractive force by 0.05 nN than on pristine graphene. In both cases, we observe that the maximum attractive force over the nearest neighbor C atom is very similar to the dopant site in the vicinity. This indicates that the short-range interaction is mostly caused by the charge transfer between the dopant and surrounding C atoms. This is not unexpected, because the B and N atoms act as donor and acceptor centers in graphene. Indeed, the presence of charge transfer is also supported by STS spectroscopy taken in the neighborhood of the B-site and pristine graphene (see Supporting Information). Nevertheless, the altered local electrostatic properties might play an important role in the interaction pathways of any polar molecules depending on their internal electrostatic charge distribution.[30]

CONCLUSIONS

We demonstrated a controlled B-doping and B,N-codoping of graphene grown on the SiC(0001) substrate. At the concentrations explored in this study, B and N dopants were found in the prevailing form of the single-atom substitutional positions. The photoelectron spectroscopy techniques proved the incorporation of the B dopants into the graphene lattice, but also suggest a diffusion of B atoms to the subsurface region. Our two-step methodology for single B-doping and BN-codoping might open new perspectives in graphene/SiC-based electronics. By using a suitable masking technique for the doping process, control of dopant distribution can be achieved. In principle, a nanoscopic p−n junction device consisting of only single B and N dopants in graphene could be manufactured using the methodology introduced here.

We performed simultaneous dAFM/STM 3D mapping of the B and N dopants. Detailed analysis of the tunneling current variation over the two different dopants supported by the theoretical calculations allowed us to attribute the characteristic tunneling current dip over the N-site to the quantum interference effect. On the B-sites, this effect was completely missing. This striking difference in the atomic contrast allows reliable chemical identification of N and B dopants in STM images. The origin of the quantum interference is related to an antibonding character of the wave function localized on the N dopant, which has a characteristic node between the central N atom and its nearest neighbor C atoms.

In addition, we analyzed local chemical properties of B- and N-sites. We found distinct interaction of the probe and the N,B dopants and graphene, which is mainly caused by local electrostatic interaction due to charge transfer from/to the dopant, respectively. The presence of the weak electrostatic force can play a significant role in graphene functionalization using polar molecules.

METHODS

The basic sample characterization microscopy was performed using an ultra-high-vacuum STM instrument, operating at room temperature, and the XPS and NEXAFS were measured at the Materials Science Beamline at Elettra synchrotron. The samples were 4.0 × 10.0 × 0.3 mm^3 stripes of n-type Si terminated 6H-SiC(0001). We mounted them into Mo sample holders designed for an *in situ* direct current heating. Single and bilayer B-doped graphene was grown using a scheme derived from the methodologies that were described elsewhere.[6,33,34] Annealing of the samples at temperatures of ∼850 °C under Si flux is crucial for efficient native oxide removal from the surface and increasing the size of atomic terraces. As an atomic source of Si and also B atoms, we used a heavily B-doped Si wafer (0.01 Ω × cm), annealed by direct current to 1200 °C. The high amount of B in the Si wafer allowed deposition of B atoms on the sample along with the flux of Si. For the XPS and the NEXAFS measurements the B concentration on the sample has been further increased by depositing pure B from an e-beam-heated B-filled graphite crucible, to surpass the detection limit of the instrument and to control the B concentration. The N-doping was achieved by ion implantation using a standard ion gun and subsequent annealing of the sample to 1100 °C. Details of the N-doping procedure are described in our previous work.[20]

For the simultaneous STM/dAFM measurements on the individual dopants and the 3D mapping, the samples were transferred into a Joule-Thomson cryostat scanning probe microscope, operating at 1.2 K. All maps have been taken at constant-height regime, and the residual drift was corrected by postprocessing. For the purposes of visualization, the 3D maps have been normalized for each tip−sample distance separately. The frequency shift curves were converted to short-range force by using the Sader formula and subtracting the long-range contribution.[35] The long-range force has been estimated for the individual dopant measurements by fitting the tails of curves taken above graphene with an inverse square dependence.

We used 8 × 8 and 18 × 18 supercells of a free-standing single-layer graphene to simulate the B-doping and BN-codoping of graphene with the DFT method. The equilibrium positions of atoms were found using a local orbital Fireball DFT code[36,37] based on an optimized pseudoatomic spd orbital basis set.[38] A very similar optimized structure was also reached with the Vienna Ab Initio Simulation Package (VASP),[39] and a plane-wave *ab initio* code using Vanderbilt ultrasoft pseudopotentials[40] was used. The plane-wave cutoff was set to 348 eV. The exchange−correlation functional was approximated with the PW91 variant of the generalized gradient approximation.[41] The Brillouin zone corresponding to the supercell was sampled with 6 × 6 k-points.

We performed STM simulations of the optimized geometries, which were done with the STM module within the Fireball code using Green's function approach.[42] A preoptimized (111)-oriented C tip with diamond-like structure was used to generate constant-height maps of current for comparison with the STM experimental images.

Conflict of Interest: The authors declare no competing financial interest.

Acknowledgment. This work has been supported by GAČR, grant nos. 14-374527G and 15-07172S. Access to computing and storage facilities owned by parties and projects contributing to the National Grid Infrastructure MetaCentrum, provided under the program "Projects of Large Infrastructure for Research, Development, and Innovations" (LM2010005), is greatly appreciated. F.C.B. acknowledges the financial support from the Initiative and Networking Fund of the Helmholtz Association, Postdoc Program VH-PD-025. M.V. was supported by the Ministry of Education of the Czech Republic under grant LM2011029.

Supporting Information Available: The Supporting Information is available free of charge on the ACS Publications website at DOI: 10.1021/acsnano.5b03690.

Large-scale STM images of samples with different concentrations of B and N, STM images showing various types of substitutional dopants, experimental STS spectra taken over B and its vicinity, and N 1s photoemission spectra taken after N ion bombardment (PDF)

REFERENCES AND NOTES

1. Geim, A. K.; Novoselov, K. S. The Rise of Graphene. *Nat. Mater.* **2007**, *6*, 183–191.
2. Geim, A. K. Graphene Status and Prospects. *Science* **2009**, *324*, 1530–1534.
3. Novoselov, K. S.; Geim, A. K.; Morozov, S. V.; Jiang, D.; Zhang, Y.; Dubonos, S. V.; Grigorieva, I. V.; Firsov, A. A. Electric Field Effect in Atomically Thin Carbon Films. *Science* **2004**, *306*, 666–669.
4. Lin, Y.-M.; Valdes-Garcia, A.; Han, S.-J.; Farmer, D. B.; Meric, I.; Sun, Y.; Wu, Y.; Dimitrakopoulos, C.; Grill, A.; Avouris, P.; et al. Wafer-Scale Graphene Integrated Circuit. *Science* **2011**, *332*, 1294–1297.
5. Lin, Y.-M.; Dimitrakopoulos, C.; Jenkins, K. A.; Farmer, D. B.; Chiu, H.-Y.; Grill, A.; Avouris, P. 100-GHz Transistors from Wafer-Scale Epitaxial Graphene. *Science* **2010**, *327*, 662.
6. Riedl, C.; Coletti, C.; Starke, U. Structural and Electronic Properties of Epitaxial Graphene on SiC(0001): a Review of Growth, Characterization, Transfer Doping and Hydrogen Intercalation. *J. Phys. D: Appl. Phys.* **2010**, *43*, 374009.
7. Chang, C.-K.; Kataria, S.; Kuo, C.-C.; Ganguly, A.; Wang, B.-Y.; Hwang, J.-Y.; Huang, K.-J.; Yang, W.-H.; Wang, S.-B.; Chuang, C.-H.; et al. Band Gap Engineering of Chemical Vapor Deposited Graphene by in Situ BN Doping. *ACS Nano* **2013**, *7*, 1333–1341.
8. Shinde, P. P.; Kumar, V. Direct Band Gap Opening in Graphene by BN Doping: Ab Initio Calculations. *Phys. Rev. B: Condens. Matter Mater. Phys.* **2011**, *84*, 125401.
9. Xu, B., Lu, Y. H., Feng, Y. P., Lin, J. Y. Density Functional Theory Study of BN-Doped Graphene Superlattice: Role of Geometrical Shape and Size. *J. Appl. Phys.* **2010**, *108*.073711
10. Zhang, Y.; Zhang, L.; Zhou, C. Review of Chemical Vapor Deposition of Graphene and Related Applications. *Acc. Chem. Res.* **2013**, *46*, 2329–2339.
11. Lu, Y.-F.; Lo, S.-T.; Lin, J.-C.; Zhang, W.; Lu, J.-Y.; Liu, F.-H.; Tseng, C.-M.; Lee, Y.-H.; Liang, C.-T.; Li, L.-J. Nitrogen-Doped Graphene Sheets Grown by Chemical Vapor Deposition: Synthesis and Influence of Nitrogen Impurities on Carrier Transport. *ACS Nano* **2013**, *7*, 6522–6532.
12. Wei, D.; Liu, Y.; Wang, Y.; Zhang, H.; Huang, L.; Yu, G. Synthesis of N-Doped Graphene by Chemical Vapor Deposition and Its Electrical Properties. *Nano Lett.* **2009**, *9*, 1752–1758.
13. Zhao, L.; He, R.; Rim, K. T.; Schiros, T.; Kim, K. S.; Zhou, H.; Gutiérrez, C.; Chockalingam, S. P.; Arguello, C. J.; Pálová, L.; et al. Visualizing Individual Nitrogen Dopants in Monolayer Graphene. *Science* **2011**, *333*, 999–1003.
14. Zhao, L.; Levendorf, M.; Goncher, S.; Schiros, T.; Pálová, L.; Zabet-Khosousi, A.; Rim, K. T.; Gutiérrez, C.; Nordlund, D.; Jaye, C.; et al. Local Atomic and Electronic Structure of Boron Chemical Doping in Monolayer Graphene. *Nano Lett.* **2013**, *13*, 4659–4665.
15. Gebhardt, J.; Koch, R. J.; Zhao, W.; Höfert, O.; Gotterbarm, K.; Mammadov, S.; Papp, C.; Görling, A.; Steinrück, H.-P.; Seyller, T. Growth and Electronic Structure of Boron-Doped Graphene. *Phys. Rev. B: Condens. Matter Mater. Phys.* **2013**, *87*, 155437.
16. Bepete, G.; Voiry, D.; Chhowalla, M.; Chiguvare, Z.; Coville, N. J. Incorporation of Small BN Domains in Graphene During CVD Using Methane, Boric Acid and Nitrogen Gas. *Nanoscale* **2013**, *5*, 6552–6557.
17. Velez-Fort, E.; Mathieu, C.; Pallecchi, E.; Pigneur, M.; Silly, M. G.; Belkhou, R.; Marangolo, M.; Shukla, A.; Sirotti, F.; Ouerghi, A. Epitaxial Graphene on 4H-SiC(0001) Grown under Nitrogen Flux: Evidence of Low Nitrogen Doping and High Charge Transfer. *ACS Nano* **2012**, *6*, 10893–10900.
18. Joucken, F.; Tison, Y.; Lagoute, J.; Dumont, J.; Cabosart, D.; Zheng, B.; Repain, V.; Chacon, C.; Girard, Y.; Botello-Méndez, A. R.; et al. Localized State and Charge Transfer in Nitrogen-Doped Graphene. *Phys. Rev. B: Condens. Matter Mater. Phys.* **2012**, *85*, 161408.
19. Bangert, U.; Pierce, W.; Kepaptsoglou, D. M.; Ramasse, Q.; Zan, R.; Gass, M. H.; Van den Berg, J. A.; Boothroyd, C. B.; Amani, J.; Hofsäss, H. Ion Implantation of Graphene - Toward IC Compatible Technologies. *Nano Lett.* **2013**, *13*, 4902–4907.
20. Telychko, M.; Mutombo, P.; Ondráček, M.; Hapala, P.; Bocquet, F. C.; Kolorenč, J.; Vondráček, M.; Jelínek, P.; Švec, M. Achieving High-Quality Single-Atom Nitrogen Doping of Graphene/SiC(0001) by Ion Implantation and Subsequent Thermal Stabilization. *ACS Nano* **2014**, *8*, 7318–7324.
21. Tison, Y.; Lagoute, J.; Repain, V.; Chacon, C.; Girard, Y.; Rousset, S.; Joucken, F.; Sharma, D.; Henrard, L.; Amara, H.; et al. Electronic Interaction between Nitrogen Atoms in Doped Graphene. *ACS Nano* **2015**, *9*, 670–678.
22. Kim, K.-j.; Yang, S.; Park, Y.; Lee, M.; Kim, B.; Lee, H. Annealing Effects after Nitrogen Ion Casting on Monolayer and Multilayer Graphene. *J. Phys. Chem. C* **2013**, *117*, 2129–2134.
23. Willke, P., Amani, J. A., Thakur, S., Weikert, S., Druga, T., Maiti, K., Hofsäss, H., Wenderoth, M. Short-Range Ordering of Ion-Implanted Nitrogen Atoms in SiC-Graphene. *Appl. Phys. Lett.* **2014**, *105*.111605
24. Willke, P.; Amani, J. A.; Sinterhauf, A.; Thakur, S.; Kotzott, T.; Druga, T.; Weikert, S.; Maiti, K.; Hofsäss, H.; Wenderoth, M. Doping of Graphene by Low-Energy Ion Beam Implantation: Structural, Electronic, and Transport Properties. *Nano Lett.* **2015**, .
25. Telychko, M.; Berger, J.; Majzik, Z.; Jelínek, P.; Švec, M. Graphene on SiC(0001) Inspected by Dynamic Atomic Force Microscopy at Room Temperature. *Beilstein J. Nanotechnol.* **2015**, *6*, 901–906.
26. Castro Neto, A. H.; Guinea, F.; Peres, N. M. R.; Novoselov, K. S.; Geim, A. K. The Electronic Properties of Graphene. *Rev. Mod. Phys.* **2009**, *81*, 109–162.
27. Blanco, J. M.; González, C.; Jelínek, P.; Ortega, J.; Flores, F.; Pérez, R. First-Principles Simulations of STM Images: From tunneling to The Contact Regime. *Phys. Rev. B: Condens. Matter Mater. Phys.* **2004**, *70*, 085405.
28. Yurtsever, A.; Sugimoto, Y.; Tanaka, H.; Abe, M.; Morita, S.; Ondracek, M.; Pou, P.; Perez, R.; Jelínek, P. Force Mapping on a Partially H-Covered Si(111)-(7 × 7) Surface: Influence of Tip and Surface Reactivity. *Phys. Rev. B: Condens. Matter Mater. Phys.* **2013**, *87*, 155403.
29. Sugimoto, Y.; Pou, P.; Abe, M.; jelinek, p.; Perez, R.; Morita, S.; Custance, O. Chemical Identification of Individual Surface Atoms by Atomic Force Microscopy. *Nature* **2007**, *446*, 64–67.

30. Kong, L.; Enders, A.; Rahman, T. S.; Dowben, P. A. Molecular Adsorption on Graphene. *J. Phys.: Condens. Matter* **2014**, *26*, 443001.
31. Cho, J.; Smerdon, J.; Gao, L.; Süzer, z.; Guest, J. R.; Guisinger, N. P. Structural and Electronic Decoupling of C60 from Epitaxial Graphene on SiC. *Nano Lett.* **2012**, *12*, 3018–3024.
32. Georgakilas, V.; Otyepka, M.; Bourlinos, A. B.; Chandra, V.; Kim, N.; Kemp, K. C.; Hobza, P.; Zboril, R.; Kim, K. S. Functionalization of Graphene: Covalent and Non-Covalent Approaches, Derivatives and Applications. *Chem. Rev.* **2012**, *112*, 6156–6214.
33. Huang, H.; Chen, W.; Chen, S.; Wee, A. T. S. Bottom-up Growth of Epitaxial Graphene on 6H-SiC(0001). *ACS Nano* **2008**, *2*, 2513–2518.
34. Hass, J.; de Heer, W. A.; Conrad, E. H. The Growth and Morphology of Epitaxial Multilayer Graphene. *J. Phys.: Condens. Matter* **2008**, *20*, 323202.
35. Sader, J. E.; Jarvis, S. P. Accurate Formulas for Interaction Force and Energy in Frequency Modulation Force Spectroscopy. *Appl. Phys. Lett.* **2004**, *84*, 1801–1803.
36. Jelinek, P.; Wang, H.; Lewis, J.; Sankey, O. F.; Ortega, J. Multicenter Approach to the Exchange-Correlation Interactions in *Ab Initio* Tight-binding Methods. *Phys. Rev. B: Condens. Matter Mater. Phys.* **2005**, *71*, 235101.
37. Lewis, J.; Jelinek, P.; Ortega, J.; Demkov, A.; Trabada, D.; Haycock, B.; Wang, H.; Adams, G.; Tomfohr, J.; Abad, E.; et al. Advances and Applications in the FIREBALL Ab Initio Tight-Binding Molecular-Dynamics Formalism. *Phys. Status Solidi B* **2011**, *248*, 1989–2007.
38. Basanta, M. A.; Dappe, Y. J.; Jelínek, P.; Ortega, J. Optimized Atomic-Like Orbitals for First-Principles Tight-Binding Molecular Dynamics. *Comput. Mater. Sci.* **2007**, *39*, 759–766.
39. Kresse, G.; Furthmüller, J. Efficient Iterative Schemes for Ab Initio Total-Energy Calculations using a Plane-Wave Basis Set. *Phys. Rev. B: Condens. Matter Mater. Phys.* **1996**, *54*, 11169–11186.
40. Vanderbilt, D. Soft Self-Consistent Pseudopotentials in a Generalized Eigenvalue Formalism. *Phys. Rev. B: Condens. Matter Mater. Phys.* **1990**, *41*, 7892–7895.
41. Perdew, J. P.; Chevary, J. A.; Vosko, S. H.; Jackson, K. A.; Pederson, M. R.; Singh, D. J.; Fiolhais, C. Atoms, Molecules, Solids, and Surfaces: Applications of the Generalized Gradient Approximation for Exchange and Correlation. *Phys. Rev. B: Condens. Matter Mater. Phys.* **1992**, *46*, 6671–6687.
42. Blanco, J.; Flores, F.; Perez, R. STM-theory: Image Potential, Chemistry and Surface Relaxation. *Prog. Surf. Sci.* **2006**, *81*, 403–443.